Probing dressed states and quantum nonlinearities in a strongly coupled three-qubit waveguide system under optical pumping

Sofia Arranz Regidor [*] and Stephen Hughes
Department of Physics, Engineering Physics and Astronomy, Queen's University, Kingston, Ontario, Canada K7L 3N6

(Received 6 October 2022; revised 17 March 2023; accepted 6 September 2023; published 27 September 2023)

We study a three-qubit waveguide system in the presence of optical pumping, when the side qubits act as atomlike mirrors, manifesting in a strong light-matter coupling regime. The qubits are modeled as two-level systems, where we account for important saturation effects and quantum nonlinearities. Optically pumping this system into a nonlinear regime is shown to lead to a rich manifold of dressed states that can be seen in the emitted spectrum, and we show two different theoretical solutions using a medium-dependent master-equation model in the Markovian limit, as well as using matrix product states without invoking any Markov approximations. We demonstrate how a rich nonlinear spectrum is obtained by varying the relative decay rates of the mirror qubits as well as their spatial separation and show the limitations of using a Markovian master equation. Our model allows one to directly model giant-atom phenomena, while including important retardation effects and multiphoton nonlinearities. We also show how the excited three-qubit system, in a strong-coupling regime, deviates significantly from a Jaynes-Cummings model when entering the nonlinear regime.

DOI: 10.1103/PhysRevA.108.033719

I. INTRODUCTION

Waveguide quantum electrodynamics (QED) is important in the study of light-matter interactions in quantum optical circuits [1], allowing a controlled coupling between two-level systems (TLSs) or quantum bits (qubits) and a continuum of quantized modes [2,3]. Waveguide QED systems give rise to new effects not observed in free-space quantum optics or in traditional cavity QED [4]. In particular, the quasi-one-dimensional confinement enhances the qubit coupling, allowing one to manipulate light-matter interactions between qubits and waveguide mode photons [5,6]. Moreover, an ensemble of qubits in a waveguide generates strongly correlated photon transport beyond the dipole-dipole interaction regime [7], allowing one to study rich many-body dynamics.

Although waveguide QED systems are excellent systems for confining photons to waveguide modes, they naturally dissipate, which can make experimental demonstrations difficult, e.g., for confining photons and realizing nonlinear resonances. Different approaches have been used in order to overcome this limitation, with the utilization of so-called giant atoms being one of the most successful proposals [8–11]. A giant-atom configuration can enable a decoherence-free interaction with waveguide QED [12–14], by manipulating the phase between different qubits in the waveguide. Various material systems can realize waveguide QED implementations, including superconducting circuits [13,15,16] and quantum dots [17–19]. Another unique feature of waveguide QED is the ability to realize and exploit non-Markovian dynamics, which can be realized with time-delayed coherent feedback and with suitably long delay times between multiple qubits [20–31].

One of the defining features of QED systems is for exploring unique quantum nonlinearities, which have no classical analog, an example of which is found in the anharmonicity of a driven Jaynes-Cummings (JC) ladder system [32–35]. At the linear-response level, vacuum Rabi oscillations can occur [36], which can also be explained classically or semiclassically [37]. Nevertheless, vacuum Rabi splitting is an important prerequisite for exploring unique quantum nonlinearities in the strong-coupling regime.

Recently, it was experimentally demonstrated how atomlike mirrors [38,39] can realize a strong light-matter coupling regime similar to a JC system, using superconducting qubits [15]. These works focused on the linear response with qubit spatial separations that are in a Markovian regime, and it is interesting to explore how such a system behaves in a nonlinear regime (which is precisely where one may find unique quantum phenomena), which challenges many of the usual quantum optics models. Specifically, how does such a finite-size cavitylike system respond when optically pumped to a nonlinear regime and does the system follow a (dissipative) JC model or an extended system of three coupled qubits? In this paper we directly address these questions by modeling an optically pumped target qubit embedded in atomlike mirrors (see Fig. 1). We explore both Markovian and non-Markovian regimes and demonstrate a host of new resonances in the nonlinear regime.

The rest of our paper is organized as follows. In Sec. II we introduce the main theoretical approaches for modeling the three-qubit waveguide system. First we present a Markovian master-equation solution and connect it to the medium-dependent Green's functions to explain the various decay rates and photonic coupling effects in a self-consistent way, using a macroscopic QED approach. For the main observable of interest, we use the waveguide-emitted spectrum,

[*]18sar4@queensu.ca

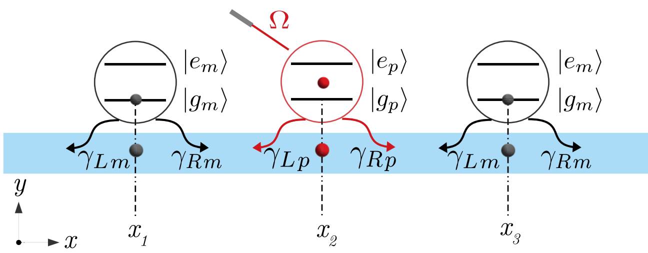

FIG. 1. Schematic of three qubits in a waveguide, with optical pumping of the middle (probe) qubit.

which contains contributions from all qubits. Second we present a matrix product state (MPS) approach, allowing us to include multiple quantized waveguide photons and fully describe non-Markovian effects, which is important when optical delays are introduced (e.g., for qubits with larger separations, when a Markov approximation is no longer valid). As a useful reference, we also show the solution for linear response, previously studied in Ref. [40].

In Sec. III we study various excitation regimes of the two theoretical models. We first highlight the linear regime, where the system also gives an analog of vacuum Rabi splitting (two polariton peaks), which can be modified further for finite separations between the qubits (when the effects of retardation become important [40]). We study the emitted spectrum as a function of the different qubit decay rates and show how various sharp resonances appear when the decay rates of the mirrors (γ_m) are greater than those of the probe qubit (γ_p). We explain the main spectral peaks, by studying the transitions between the quasienergy levels (dressed states) from the system Hamiltonian, including the effect of the drive. We subsequently explore how the spectrum changes as a function of pump strength, and explain the resonance features in terms of allowed transitions between dressed states. We compare these findings with the solutions of a driven JC system and demonstrate how the nonlinear features of the three qubits emerge and survive even for large pump strengths, showing features that are significantly different from the driven JC model. Next we study the waveguide QED system using the MPS approach and investigate the role of retardation, and highlight new nonlinear resonance energies for larger qubit separations. A summary and our conclusions are presented in Sec. IV.

II. THEORY

In this section we describe two different approaches to model the dynamics of the multiqubit waveguide system. First we use a Markovian master-equation approach that is derived from a macroscopic Green's-function formalism [41–44]. For a recent review of waveguide QED, including common theory techniques, see Ref. [4]. As discussed in Ref. [40], these macroscopic approaches fully recover model Hamiltonian formalisms for waveguide QED in the appropriate limit [20,38]. Second we use an MPS approach [45,46], which does not rely on the Markov approximation and can model multiphoton states in the waveguide. The MPS approach also allows us to model the effects of retardation, which is known to be important for longer qubit separations and delay times. Indeed, longer delay times are known to tune and improve the strong-coupling regime [40] at the vacuum level, and below we will investigate what happens in an optical pumping regime beyond weak excitation. For reference, we also show the frequency-dependent solution for linear response [40].

A. Markovian master equation using the waveguide Green's function

The photonic Green's function for the waveguide medium has the general analytic form [18,40]

$$\begin{aligned}\mathbf{G} &\equiv \mathbf{G}_W(\mathbf{r}_a, \mathbf{r}_b, \omega)\\ &= iA[\mathbf{f}_k(\mathbf{r}_a)\mathbf{f}_k^*(\mathbf{r}_b)H(x_a - x_b)e^{ik(x_a-x_b)}\\ &\quad + \mathbf{f}_k^*(\mathbf{r}_a)\mathbf{f}_k(\mathbf{r}_b)H(x_b - x_a)e^{ik(x_b-x_a)}],\end{aligned} \tag{1}$$

where A is a constant, $\mathbf{f}_k(\mathbf{r})$ is the waveguide mode of interest, H is the Heaviside function, and the modes at the qubit locations can be of arbitrary polarization, typically linearly polarized or circularly polarized [47,48]. Note that $\mathbf{G}$ is a dyad, formed by the outer product of two vectors, but in general we can consider a single component of interest, where the dipoles of the emitters are aligned with the mode polarization. Thus, if $x_a > x_b$, then $G_W(\mathbf{r}_a, \mathbf{r}_b, \omega) = iAe^{i\omega\tau_{ab}}$ (where we choose the relative polarization component), and τ_{ab} is the delay time to propagate from point $\mathbf{r}_a$ to point $\mathbf{r}_b$. Note that the wave vector is dispersive in general, so $k = k(\omega)$.

Using a photonic Green's-function approach for the waveguide system, a Lindblad master equation can be derived within a Markov approximation [41,42]

$$\begin{aligned}\dot{\rho}(t) = &-\frac{i}{\hbar}[H_{\rm S}, \rho(t)] - i\sum_{n,n'}^{n\neq n'}\delta_{nn'}[\sigma_n^+\sigma_{n'}^-, \rho(t)]\\ &+\sum_{n,n'}\frac{\Gamma_{nn'}}{2}[2\sigma_{n'}^+\rho(t)\sigma_n^- - \rho(t)\sigma_n^-\sigma_{n'}^+ - \sigma_n^-\sigma_{n'}^+\rho(t)],\end{aligned} \tag{2}$$

where the various coupling rates are defined below. In this approach, the waveguide is treated as a reservoir, so waveguide photons are assumed to be uncorrelated with the qubits, and $\sigma_n^{\pm}$ are the usual Pauli operators for the qubits treated as TLSs, each with a dipole moment $\mathbf{d}_n$.

To solve the Markovian master equation, we first define the incoherent scattering rates used in the Lindbladian, which are obtained from the medium Green's function,

$$\Gamma_{ab}|_{a\neq b} = \frac{2\mathbf{d}_a \cdot {\rm Im}\mathbf{G}(\mathbf{r}_a, \mathbf{r}_b, \omega_b) \cdot \mathbf{d}_b}{\epsilon_0\hbar}, \tag{3}$$

$$\gamma_a \equiv \Gamma_{aa} = \frac{2\mathbf{d}_a \cdot {\rm Im}\mathbf{G}(\mathbf{r}_a, \mathbf{r}_a, \omega_a) \cdot \mathbf{d}_a}{\epsilon_0\hbar}, \tag{4}$$

where the latter term is the usual spontaneous emission rate from a single emitter and the former term accounts for interqubit photon transfer. Using the waveguide Green's functions and considering three qubits (1-mirror, 2-probe, and

3-mirror), we have

$$\begin{aligned}\Gamma_{12} &= \Gamma_{21} = \sqrt{\gamma_m\gamma_p}\,\mathrm{Re}(e^{i\phi_{m_1,p}}),\\ \Gamma_{13} &= \Gamma_{31} = \gamma_m \mathrm{Re}(e^{i\phi_{m_1,m_2}}),\\ \Gamma_{23} &= \Gamma_{32} = \sqrt{\gamma_m\gamma_p}\,\mathrm{Re}(e^{i\phi_{m_2,p}}),\end{aligned} \tag{5}$$

where $\phi_{m_1,p}$, $\phi_{m_2,p}$, and ϕ_{m_1,m_2} represent the phases between the qubits in the waveguide. Explicitly, $\phi_{n,n'} = k(x_n - x_{n'})$, which is also frequency dependent. The coherent coupling rates are obtained from the real part of the Green's functions,

$$\delta_{ab}|_{a\neq b} = -\frac{2\mathbf{d}_a \cdot \mathrm{Re}\mathbf{G}(\mathbf{r}_a, \mathbf{r}_b, \omega_b)\cdot \mathbf{d}_b}{2\epsilon_0\hbar}, \tag{6}$$

which, for the waveguide system, simplifies to

$$\begin{aligned}\delta_{12} &= \delta_{21} = \sqrt{\gamma_m\gamma_p}\,\mathrm{Im}(e^{i\phi_{m_1,p}}),\\ \delta_{13} &= \delta_{31} = \gamma_m \mathrm{Im}(e^{i\phi_{m_1,m_2}}),\\ \delta_{23} &= g_{32} = \sqrt{\gamma_m\gamma_p}\,\mathrm{Im}(e^{i\phi_{m_2,p}}).\end{aligned} \tag{7}$$

The effective system Hamiltonian, including qubit-qubit coupling mediated by the waveguide, is then

$$\begin{aligned}H_{\mathrm{S}}^{\mathrm{eff}} = &\frac{\sqrt{\gamma_m\gamma_p}}{2}\mathrm{Im}(e^{i\phi_{m_1,p}})\big(\sigma_{m_1}^+\sigma_p^- + \sigma_p^+\sigma_{m_1}^-\big)\\ &+ \frac{\sqrt{\gamma_m\gamma_p}}{2}\mathrm{Im}(e^{i\phi_{m_2,p}})\big(\sigma_{m_2}^+\sigma_p^- + \sigma_p^+\sigma_{m_2}^-\big)\\ &+ \frac{\gamma_m}{2}\mathrm{Im}(e^{i\phi_{m_1,m_2}})\big(\sigma_{m_1}^+\sigma_{m_2}^- + \sigma_{m_2}^+\sigma_{m_1}^-\big)\\ &+ \Omega(\sigma_p^- + \sigma_p^+) + \Delta_n\big(\sigma_{m_1}^+\sigma_{m_1}^- + \sigma_p^+\sigma_p^- + \sigma_{m_2}^+\sigma_{m_2}^-\big),\end{aligned} \tag{8}$$

with a possible pump Rabi field Ω exciting the probe qubit, and we also introduced a laser-qubit detuning $\Delta_n = \omega_n - \omega_L$, where $\omega_n = \omega_0$ (same for all qubits) and ω_L is the frequency of the pump. Thus, we can write the Markovian master equation as

$$\begin{aligned}\dot{\rho}(t) = &-\frac{i}{\hbar}[H_{\mathrm{S}}^{\mathrm{eff}}, \rho(t)]\\ &+ \sum_{n,n'}\frac{\Gamma_{nn'}}{2}[2\sigma_{n'}^+\rho(t)\sigma_n^- - \rho(t)\sigma_n^-\sigma_{n'}^+ - \sigma_n^-\sigma_{n'}^+\rho(t)].\end{aligned} \tag{9}$$

The detected spectrum at $\mathbf{r}_D$ can be obtained from the the first-order quantum correlation function $G^{(1)}(\mathbf{r}_D, \tau) = \langle \hat{\mathbf{E}}^-(\mathbf{r}_D, t)\hat{\mathbf{E}}^+(\mathbf{r}_D, t+\tau)\rangle$. In the rotating frame at the laser frequency, the total spectrum is

$$\begin{aligned}S_D^T(\omega) = &\lim_{T\to\infty}\frac{1}{T}\int_0^T dt\\ &\times \int_0^T dt' \langle \hat{\mathbf{E}}^-(\mathbf{r}_D, t)\hat{\mathbf{E}}^+(\mathbf{r}_D, t')\rangle e^{i(\omega_L-\omega)(t-t')}.\end{aligned} \tag{10}$$

Inserting the formal solution for the electric-field operator, obtained from Heisenberg's equation of motion [42], then

$$\langle \hat{\mathbf{E}}^-(\mathbf{r}_D, \omega)\hat{\mathbf{E}}^+(\mathbf{r}_D, \omega)\rangle = \sum_{n,n'} g_{n,n'}(\omega)\langle \sigma_n^+(\omega)\sigma_{n'}^-(\omega)\rangle, \tag{11}$$

where the emitter coupling term is

$$g_{n,n'}(\omega) = \frac{1}{\epsilon_0^2}\mathbf{d}_n \cdot \mathbf{G}^*(\mathbf{r}_n, \mathbf{r}_D, \omega)\cdot \mathbf{G}(\mathbf{r}_D, \mathbf{r}_{n'}, \omega)\cdot \mathbf{d}_{n'} \tag{12}$$

and $g_{n',n} = g_{n,n'}^*$.

The incoherent spectrum can be separated into direct contributions and interference terms so that ($\mathbf{r}_D$ is implicit)

$$\begin{aligned}S_D(\omega) = &\sum_n \left|\mathbf{G}(\mathbf{r}_D, \mathbf{r}_n, \omega)\cdot\frac{\mathbf{d}_n}{\epsilon_0}\right|^2 \mathrm{Re}\big(S_{n,n}^0(\omega)\big)\\ &+ \sum_{n,n'}^{n\neq n'} \mathrm{Re}\big(g_{n,n'}(\omega)S_{n,n'}^0(\omega)\big),\end{aligned} \tag{13}$$

with

$$\begin{aligned}S_{n,n'}^0(\omega) = \lim_{t\to\infty}\int_0^\infty &dt'[\langle \sigma_n^+(t+t')\sigma_{n'}^-(t)\rangle\\ &- \langle \sigma_n^+(t)\rangle\langle \sigma_{n'}^-(t)\rangle]e^{-i(\omega-\omega_L)t'},\end{aligned} \tag{14}$$

where the latter contribution subtracts the coherent spectrum, which is simply a Dirac delta function for continuous-wave pumping. Full derivations of the master equation and spectra are presented in Refs. [41,42].

We recognize that the total spectrum contains terms corresponding to the spectrum emitted from the single qubits ($n = n'$), as well as interference terms ($n \neq n'$). Finally, to be consistent with the Markov approximation used in the master equations, we replace $\mathbf{G}(\mathbf{r}_D, \mathbf{r}_n, \omega)$ by $\mathbf{G}(\mathbf{r}_D, \mathbf{r}_n, \omega_L)$, though this is not a model requirement.

B. Matrix product states

For the MPS approach, we can write our state as

$$|\psi\rangle = \sum_{i_s i_1\cdots i_N} A_{a_1}^{i_s}A_{a_1,a_2}^{i_1}\cdots A_{a_{N-1},a_N}^{i_{N-1}}A_{a_N}^{i_N}\,|i_s, i_1, \ldots, i_N\rangle, \tag{15}$$

where i_s represents the system bin containing the three TLSs and the remaining $i_1, \ldots, i_N$ terms represent the discretized waveguide. Here each of the A terms is a tensor where the subscripts $a_1, \ldots, a_{N-1}$ are the auxiliary dimensions of each element and the superscripts $i_1, \ldots, i_N$ represent the physical dimensions of the system [45].

Setting the units such that $\hbar = 1$ for convenience, we consider the total Hamiltonian

$$H = H_{\mathrm{sys}} + H_{\mathrm{B}} + H_{\mathrm{int}}, \tag{16}$$

where

$$H_{\mathrm{sys}} = \sum_{n=m_1,p,m_2}\left[\omega_n\sigma_n^+\sigma_n^- - \frac{1}{2}(\Omega_n\sigma_n^- e^{i\omega_L t} + \mathrm{H.c.})\right], \tag{17}$$

$$H_{\mathrm{B}} = \sum_{i=L,R}\int_B d\omega\,\omega b_i^\dagger(\omega)b_i(\omega), \tag{18}$$

$$H_{\mathrm{int}} = i\sum_{i,n}\int_B d\omega[\kappa_i(\omega)b_i^\dagger(\omega)\sigma_n^- e^{-i\omega x_i/v_i} - \mathrm{H.c.}]. \tag{19}$$

Switching to the interaction picture with respect to the bath Hamiltonian and into a rotating frame with the frequency ω_L, then

$$H_{\rm sys} = \sum_{n=m_1,p,m_2} \left[\Delta_n \sigma_n^+ \sigma_n^- - \frac{1}{2}(\Omega_n \sigma_n^- + {\rm H.c.}) \right]. \tag{20}$$

Next, choosing $\kappa_i \rightarrow \sqrt{\gamma_i/2\pi}$, then

$$H_{\rm int} = \frac{i}{\sqrt{2\pi}} \sum_{i,n} \int_B d\omega [\sqrt{\gamma_i} b_i^\dagger(\omega) \sigma_n^- e^{-i\omega x_i/v_i} e^{i(\omega-\omega_L)t} - {\rm H.c.}]. \tag{21}$$

If we choose $x = 0$ for the middle dot, then we can define $x_1 = -x$, $x_2 = 0$, and $x_3 = x$. The group velocity of the waveguide mode is considered constant (over the bandwidth of interest), with $v_L = -v$ and $v_R = v$.

The delay time between the probe dot and the mirror dot (τ_{pm} for our symmetric system) is redefined as $\tau_{pm} \equiv \tau_m$ and $\tau_m = x/v$. The boson operators in the time domain are

$$b_i^\dagger(t) = \frac{1}{\sqrt{2\pi}} \int d\omega\, b_i^\dagger(\omega) e^{i(\omega-\omega_L)t},$$
$$b_i^\dagger(t-\tau_m) = \frac{1}{\sqrt{2\pi}} \int d\omega\, b_i^\dagger(\omega) e^{i(\omega-\omega_L)(t-\tau_m)},$$
$$b_i^\dagger(t+\tau_m) = \frac{1}{\sqrt{2\pi}} \int d\omega\, b_i^\dagger(\omega) e^{i(\omega-\omega_L)(t+\tau_m)}, \tag{22}$$

with corresponding equations for $b_i(t)$, $b_i(t-\tau_m)$, and $b_i(t+\tau_m)$. Thus, we can write

$$\begin{aligned} -iH_{\rm int} = &\sqrt{\gamma_L} b_L^\dagger(t-\tau_m)\sigma_{m_1}^- e^{i\omega_L\tau_m} + \sqrt{\gamma_R} b_R^\dagger(t+\tau_m)\sigma_{m_1}^- e^{-i\omega_L\tau_m} \\ &- \sqrt{\gamma_L} b_L(t-\tau_m)\sigma_{m_1}^+ e^{-i\omega_L\tau_m} + \sqrt{\gamma_R} b_R(t+\tau_m)\sigma_{m_1}^+ e^{i\omega_L\tau_m} \\ &+ \sqrt{\gamma_L} b_L^\dagger(t)\sigma_p^- + \sqrt{\gamma_R} b_R^\dagger(t)\sigma_p^- - \sqrt{\gamma_L} b_L(t)\sigma_p^+ + \sqrt{\gamma_R} b_R(t)\sigma_p^+ \\ &+ \sqrt{\gamma_L} b_L^\dagger(t+\tau_m)\sigma_{m_2}^- e^{-i\omega_L\tau_m} + \sqrt{\gamma_R} b_R^\dagger(t-\tau_m)\sigma_{m_2}^- e^{i\omega_L\tau_m} \\ &- \sqrt{\gamma_L} b_L(t+\tau_m)\sigma_{m_2}^+ e^{i\omega_L\tau_m} + \sqrt{\gamma_R} b_R(t-\tau_m)\sigma_{m_2}^+ e^{-i\omega_L\tau_m}. \end{aligned} \tag{23}$$

Finally, we can redefine the boson operators, choosing $t + \tau_m \rightarrow t'$, and define the phases between dots as in Sec. II A (i.e., $\omega_L\tau_m = \phi_{m1,p} = \phi_{m1,p} = \phi_{m,p}$ phases between a mirror qubit and the probe qubit and $\omega_L\tau_m = \phi_{m1,m2}$ phases between mirrors). Using these in Eq. (23), we get to the final equation for the interaction Hamiltonian (and we drop the prime superscript in t'),

$$\begin{aligned} H_{\rm int}/i = &\sqrt{\gamma_L} b_L^\dagger(t-2\tau_m)\sigma_{m_1}^- + \sqrt{\gamma_R} b_R^\dagger(t)\sigma_{m_1}^- e^{-i\phi_{m1,m2}} \\ &- \sqrt{\gamma_L} b_L(t-2\tau_m)\sigma_{m_1}^+ + \sqrt{\gamma_R} b_R(t)\sigma_{m_1}^+ e^{i\phi_{m1,m2}} \\ &+ \sqrt{\gamma_L} b_L^\dagger(t-\tau_m)\sigma_p^- e^{-i\phi_{m,p}} + \sqrt{\gamma_R} b_R^\dagger(t-\tau_m)\sigma_p^- e^{-i\phi_{m,p}} \\ &- \sqrt{\gamma_L} b_L(t-\tau_m)\sigma_p^+ e^{i\phi_{m,p}} + \sqrt{\gamma_R} b_R(t-\tau_m)\sigma_p^+ e^{i\phi_{m,p}} \\ &+ \sqrt{\gamma_L} b_L^\dagger(t)\sigma_{m_2}^- e^{-i\phi_{m1,m2}} + \sqrt{\gamma_R} b_R^\dagger(t-2\tau_m)\sigma_{m_2}^- \\ &- \sqrt{\gamma_L} b_L(t)\sigma_{m_2}^+ e^{i\phi_{m1,m2}} + \sqrt{\gamma_R} b_R(t-2\tau_m)\sigma_{m_2}^+. \end{aligned} \tag{24}$$

The spectrum of the output field, just after the right mirror dot, in steady state, is obtained from

$$S(\omega) \rightarrow 2\mathcal{R} \int_0^\infty dt' \langle b^\dagger(t) b(t-t') \rangle e^{i(\omega-\omega_L)t'}, \tag{25}$$

which can be written in the discrete-time bin scheme [45] as

$$S_{i,j}(\omega) \rightarrow 2\mathcal{R} \frac{1}{\Delta t} \sum_{p=0}^{M-1} \langle \Delta B^\dagger(t_q) \Delta B(t_{q-p}) \rangle e^{i(\omega-\omega_L)p\Delta t}, \tag{26}$$

where $q = k_{\rm max} - l - 1$ (with $l = \tau/\Delta t$ and $k_{\rm max}$ the last time bin) and $p \in \{0, M-1\}$ with M large enough to resolve the spectrum. This value will vary for each specific simulation case, depending on the required Δt and the necessary time to resolve the photon correlation signal. In general, we will need a smaller Δt for a small retardation and a large pump, and a longer correlation time $t_{\rm cor}$ for a large retardation. Note that $M = 1600$ is a typical value used in our calculations for an intermediate case where $\Delta t = 0.025\gamma_p$ and $t_{\rm cor} = 40\gamma_p$. All results are carefully checked for numerical convergence.

C. Exact solution for the probe-qubit electric field under linear response

For reference, here we briefly discuss the linear regime solution [40]. Defining the distance between the mirror dots as L, it is possible to derive an exact solution for the scattered electric field at the probe qubit in a weak-excitation approximation (namely, under linear response)

$$\tilde{E}_{\rm s}(\mathbf{r}_p, \omega) = \frac{i\omega_p \tilde{\gamma}_p}{\omega_p^2 - \omega^2 - i\omega\tilde{\gamma}_p}, \tag{27}$$

where all qubits are on-resonance and the modified decay rate is defined from [40]

$$\begin{aligned} \tilde{\gamma}_p = \gamma_p \Bigg(&1 + e^{ikL} r_1(\omega) + [e^{ikL/2} + e^{ikL/2} e^{ikL} r_1(\omega)] \\ &\times \frac{r_1(\omega)(e^{ikL/2} + r_1(\omega) e^{ikL/2} e^{ikL})}{1 - r_1^2(\omega) e^{2ikL}} \Bigg), \end{aligned} \tag{28}$$

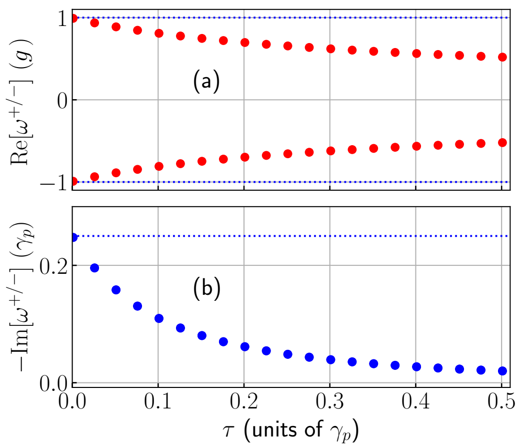

FIG. 2. Complex poles of the two main polariton states calculated using Eq. (27), with $\tau = 2\tau_m$ the delay time between mirror qubits and $\gamma_m = 10\gamma_p$. The dashed lines show the nonretarded solution (Markov limit).

and we use the single-qubit reflection coefficient

$$r_1(\omega) = \frac{\mathbf{E}_{\mathrm{r}}(\mathbf{r}; x \to -\infty)}{\mathbf{E}^{\mathrm{h}}(\mathbf{r}; x \to -\infty)} = \frac{i\omega_0 \gamma e^{i\phi(x_d)}}{\omega_0^2 - \omega^2 - i\omega_0\gamma}, \tag{29}$$

where $\phi(x_d)$ is a positional-dependent phase. Using the mirror qubits, then $\gamma = \gamma_m$. Clearly this solution contains multiple resonances. With an appropriate choice for the decay rates, one can achieve an analog of vacuum Rabi splitting for the main two polariton peaks, when $g > \gamma_m$, where $g = \sqrt{2\gamma_m\gamma_p}/2$. However, this limit is only achieved in the Markovian regime. In the same limit, the broadening of these peaks is $\gamma_p/4$, which can be compared with $\kappa/2$ from the usual cavity QED system in the absence of vertical (background) decay [49].

III. RESULTS

A. Linear response of the vacuum Rabi polariton poles for different delay times

As shown in Ref. [40], retardation effects can have a significant influence on the coupling rate of this cavitylike system. This linear result is shown in Fig. 2, where the first near-resonant complex poles are calculated as a function of the delay time. However, note that the general solution contains multiple resonances. We observe how the values of the complex poles decrease for an increasing retardation time. The frequency units are shown in terms of a derived cavity-atom coupling rate g. We stress that this coupling rate is only valid for small delay times, and general, the resonances depend on the distance between the qubits. Hence, later will consider an effective coupling rate $g_{\mathrm{eff}} < g$, when one enters a non-Markovian regime, as the Rabi doublets decrease in energy and spectrally sharpen.

It is important to realize that these non-Markovian delay times correspond to much longer length scales than a few wavelengths. For example, if we consider a delay time of $\tau = 0.2/\gamma_p$, with a typical quantum-dot (QD) decay rate $\gamma_p = 1\ \mathrm{ns}^{-1}$ and a group index $n_g = c/v_g = 10$, the distance between the probe qubit and the mirror one will be 6 mm, which is thousands of wavelengths for typical integrated quantum dots (e.g., with a wavelength of 1000 nm). Thus, low-loss waveguides are required, such as SiN [50].

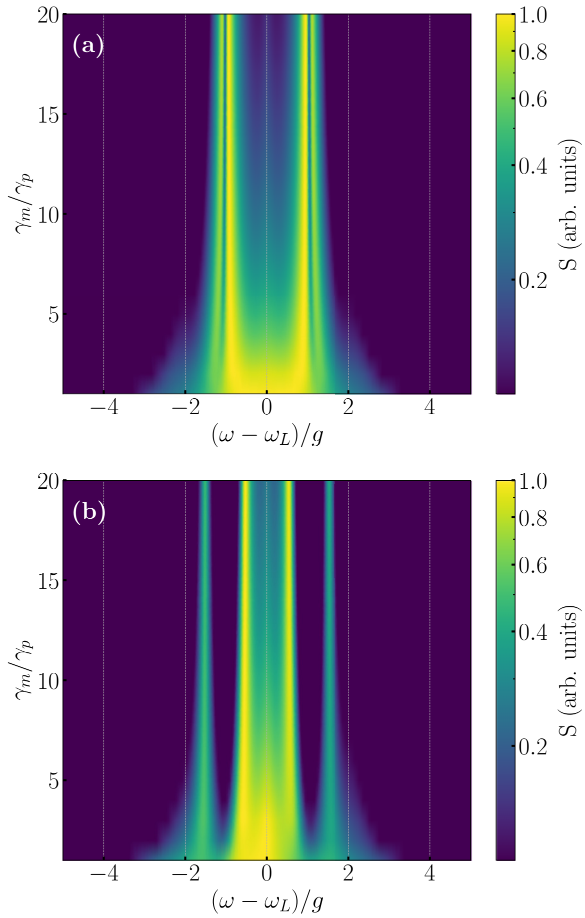

FIG. 3. Master-equation calculation of the total spectrum of a three-qubit system for different ratios of γ_m/γ_p in the Markovian (nonretarded) regime. The probe dot is pumped with $\Omega = 0.5\gamma_p \approx 0.22g$: (a) on-resonance pumping and (b) off-resonance pumping with $\Delta_n = g/2$.

B. Nonlinear Markovian regime

1. Emitted spectrum for different qubit decay rate ratios

We next solve the three-qubit Markovian master equation [Eq. (2)] and investigate the analog of a cavity QED system by using the side qubits acting as dipole mirrors [15] (through resonant scattering) but now with optical pumping. All the calculations presented are performed in PYTHON, and for this first method, we make use of the QuTiP library [51,52]. For the excitation, we pump the center TLS (probe qubit) with a sufficiently strong field $\Omega = 0.5\gamma_p$, so as to induce nonlinear interactions, and study the influence of the ratio γ_m/γ_p. Using resonant pumping, in Fig. 3(a) we show how, by increasing the γ_m/γ_p ratio, the total spectrum [Eq. (13)] of our system resembles the characteristic Rabi splitting from a cavity system when pumped on-resonance (as also shown in Fig. 2), under linear response. Note that if we go to the opposite limit, where $\gamma_m/\gamma_p \approx 0$, then the system

TABLE I. Dressed state labels with coherent qubit interactions and the correspondence in terms of the bare states.

Dressed state	Correspondence in bare basis
$\|0\rangle$	$\|ggg\rangle$
$\|1_a\rangle$	$\frac{1}{\sqrt{2}}\|geg\rangle - \frac{1}{2}(\|egg\rangle + \|gge\rangle)$
$\|1_b\rangle$	$\frac{1}{\sqrt{2}}(\|egg\rangle - \|gge\rangle)$
$\|1_c\rangle$	$\frac{1}{\sqrt{2}}\|geg\rangle + \frac{1}{2}(\|egg\rangle + \|gge\rangle)$
$\|2_a\rangle$	$\frac{1}{\sqrt{2}}\|ege\rangle - \frac{1}{2}(\|eeg\rangle + \|gee\rangle)$
$\|2_b\rangle$	$\frac{1}{\sqrt{2}}(\|gee\rangle - \|eeg\rangle)$
$\|2_c\rangle$	$\frac{1}{\sqrt{2}}\|ege\rangle + \frac{1}{2}(\|eeg\rangle + \|gee\rangle)$
$\|3\rangle$	$\|eee\rangle$

behaves as a single TLS, since the coupling of the side dots in this limit is negligible [53].

Based on these solutions, we choose a ratio of $\gamma_m/\gamma_p = 10$ for the rest of our investigations. This regime has also been experimentally demonstrated [15], though our findings below are quite general.

Within the Markovian limit of the model, we see four resonances that show a splitting near the expected one-photon JC resonances (first photon ladder states, near $\pm g$). This indicates that we are beyond the weak-excitation limit where nonlinear effects appear from the pump field. The origin of these multiple resonances will be explained below in terms of the dressed states (Sec. III B 2).

Next, in Fig. 3(b) we show a similar study where the three qubits are still on-resonance with each other, but now we have an off-resonant pumping, with $\Delta_n = g/2$. In this case, we can again see four resonances, but they now move farther from the expected linear one-photon resonances due to the detuning introduced in the system. We now clearly see additional nonlinear states that are not associated with the linear polariton states at $\pm g$.

2. Dressed-state picture

To better explain the additional resonances that appear in the nonlinear regime, it is useful to use a dressed-state basis [54,55]. In the bare basis, we have the states $|ggg\rangle$, $|egg\rangle$, $|geg\rangle$, $|eeg\rangle$, $|gge\rangle$, $|ege\rangle$, $|gee\rangle$, and $|eee\rangle$, where g and e correspond

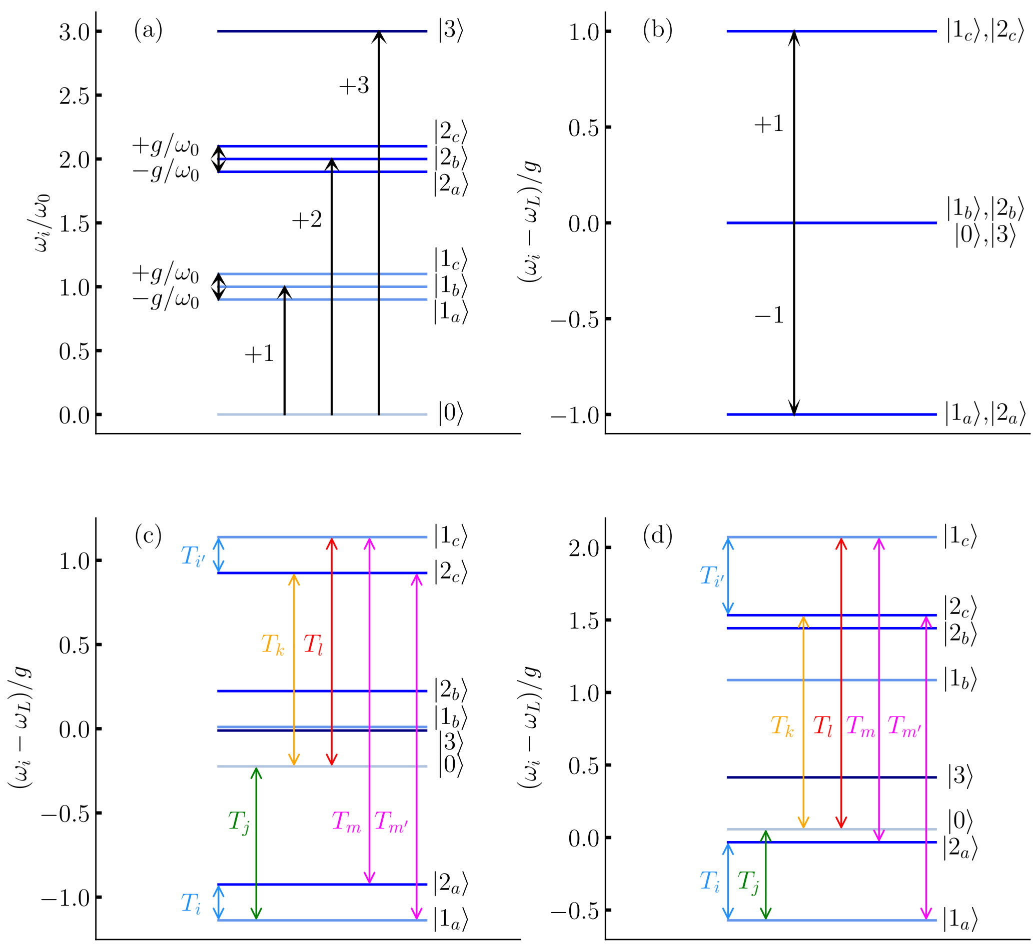

FIG. 4. Energy levels of the three-qubit system in a Markovian regime. (a) Dressed-state basis in the absence of an optical pumping without using the interaction picture. (b) Same case as in (a) but now in the interaction picture. (c) Optically driven case with $\Omega = 0.5\gamma_p \approx 0.22g$ (on-resonance). (d) Optically driven case with $\Omega = 0.5\gamma_p \approx 0.22g$ and $\Delta_n = g/2$ (off-resonance). Prime labeled transitions are degenerate with their corresponding unprimed transition. This schematic only applies to the Markovian system, and in the MPS approach there are also multiphoton states.

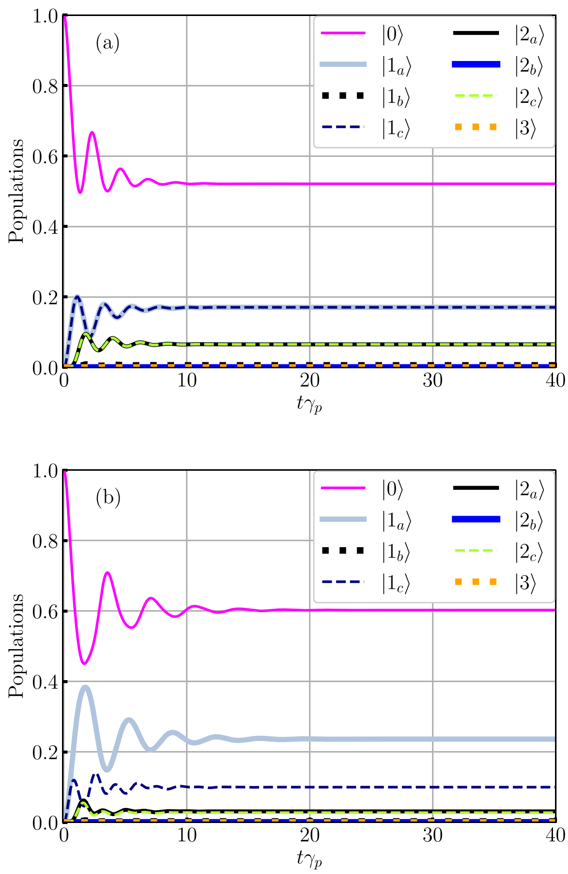

FIG. 5. Dressed-state population for $\Omega = 0.5g$ (a) on-resonance and (b) off-resonance with a detuning of $\Delta_n = g/2$.

to the ground and excited levels, respectively, of the mirror-1 qubit, probe qubit, and mirror-2 qubits. In the presence of coherent qubit interactions, we can obtain the dressed states from Eq. (8), as shown in Table I. These are the natural dressed states in the absence of any optical pumping, mediated by the coherent coupling between the qubits. Optical pumping will cause additional dressing.

In Figs. 4(a) and 4(b) we show the energy levels in the natural (unpumped) dressed-state basis without using the interaction picture and its equivalence within the interaction picture. Then in Figs. 4(c) and 4(d) we demonstrate how the states are additionally dressed by the optical pump field (on- and off-resonance, respectively) with their corresponding energy levels shifted. Key optical transitions are shown with arrows.

We also examine the emitted spectra for different pump strengths and relate the spectral peaks with the possible energy transitions between these dressed states. In order to identify the possible energy transitions that are optically allowed (from a fairly high number), we first calculate the dressed-state populations in the natural dressed-state basis, as shown in Fig. 5. In both the resonant and detuned cases, we find five populated states, which allow us to identify the dominant transitions, which are then plotted with the numerically computed spectra shown in Fig. 6 (dashed curves).

Figure 6(a) shows the spectra for on-resonance excitation. If we focus on the positive (blue) frequency side of the spectra, we can distinguish five different peaks that are labeled as T_i,

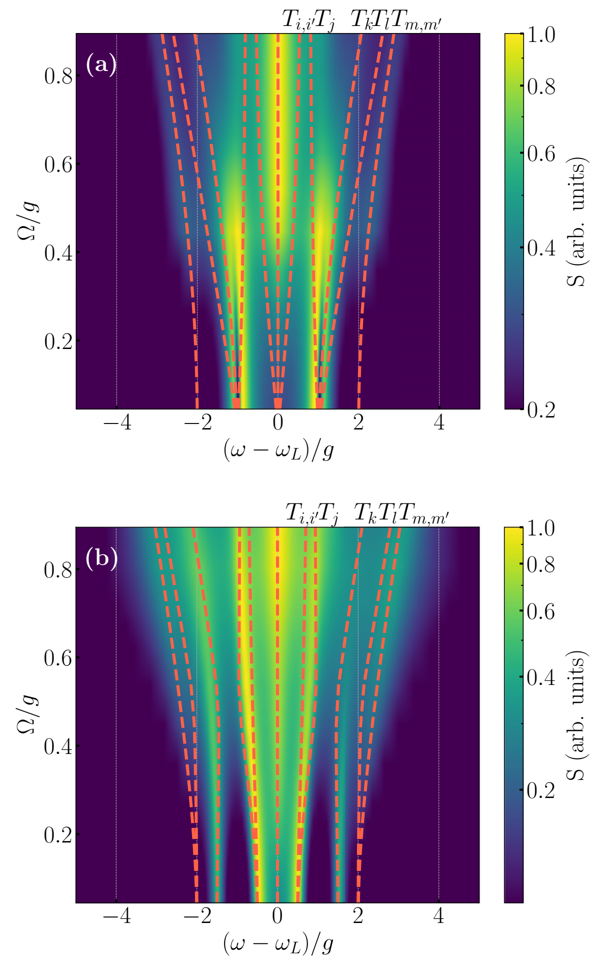

FIG. 6. Master-equation calculations [Eq. (13)] of the output spectrum of a three-qubit system for different pumping rates of the probe dot ($\gamma_m/\gamma_p = 10$). (a) On-resonance pumping. (b) Off-resonance with $\Delta_n = g/2$. Red dashed lines correspond to the transition lines shown in Fig. 4, and $T_{m,m'}$ and $T_{i,i'}$ correspond to degenerate transitions $T_m = T_{m'}$ and $T_i = T_{i'}$, respectively.

$T_{i'}$, T_j, T_k, T_l, T_m, and $T_{m'}$. These correspond directly to the transitions shown in Figs. 4(c) and 4(d), similarly labeled, plus the primed transitions which correspond to the degenerate states. Clearly, the correspondence between the full spectral results and the identified dressed-state resonances is very good.

Figure 6(b) shows the case in which the laser is off-resonance with respect to the qubits, with a detuning of $\Delta_n = g/2$. A similar dressed energy-level ladder state scheme to Fig. 6(a) is seen, but the position of the peaks observed in the spectrum are now qualitatively different due to different nonlinear dressing. However, the same basic photon transitions are identified in both scenarios.

3. Driven Jaynes-Cummings system

It is useful to also compare the nonlinear response of the three-qubit system with a driven JC system since both these systems have a similar linear response. Moreover, a key aspect of using mirror qubits is that they are fermionic systems and one can expect significantly different nonlinear interactions,

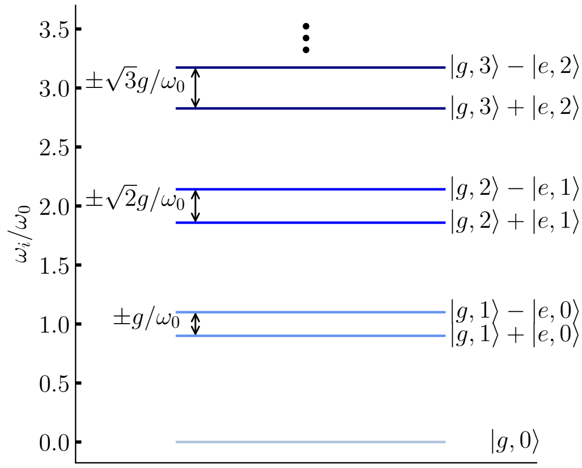

FIG. 7. Jaynes-Cummings model energy levels (of the first photon-matter states) where ω_i is the frequency of the ith eigenenergy. The qubit and cavity are on-resonance. The one-photon states yield a similar strong-coupling regime to the three-qubit system, as shown in Fig. 4(a).

even when they are behaving as mirrors for cavity QED. Thus, below we show the main features of a (dissipative) JC model which solves a single TLS interacting with a single quantized electromagnetic field mode, in the usual rotating-wave approximation [56].

For this model, we solve the corresponding master equation, following an approach similar to the one described in Sec. II A, where now the effective system Hamiltonian is [57]

$$H_S^{\rm eff} = \Delta_a(\sigma^+\sigma^-) + \Delta_c(a^\dagger a) + g(a\sigma^+ + a^\dagger\sigma^-) + \Omega(\sigma^- + \sigma^+), \qquad (30)$$

with σ^+ and σ^- the creation and annihilation operators of the single qubit, $a^\dagger$ and a the (bosonic) ladder operators of the cavity, and g the qubit-cavity coupling. As in the previous examples, Ω is the drive strength of the qubit and, in this JC case, $\Delta_a = \omega_a - \omega_L$ and $\Delta_c = \omega_c - \omega_L$ represent possible detunings between the drive and the atom or cavity, respectively. This is a standard driven JC model with an optical pumping term. In addition, we also include one collapse operator for the cavity mode decay,

$$C = \sqrt{\kappa}a, \qquad (31)$$

where κ is the cavity decay rate. Similar to the three-qubit case studied before, we assume there are no additional decay rates (e.g., off chip), other than to the waveguide or to the cavity, and so we assume κ is the dominant decay process.

The cavity-emitted spectrum is obtained from

$$S_{\rm cav}(\omega) = {\rm Re}\int_0^\infty \langle a^\dagger(t_{\rm ss})a(t_{\rm ss}+\tau)\rangle\, e^{i(\omega-\omega_L)}d\tau, \qquad (32)$$

where $t_{\rm ss}$ refers to steady state. For all the driven JC calculations below, we have carefully checked for numerical convergence by increasing the photon-number states up to a maximum of $N = 100$.

Figure 7 shows the familiar JC energy-level ladder system for the dressed states, in the absence of optical pumping.

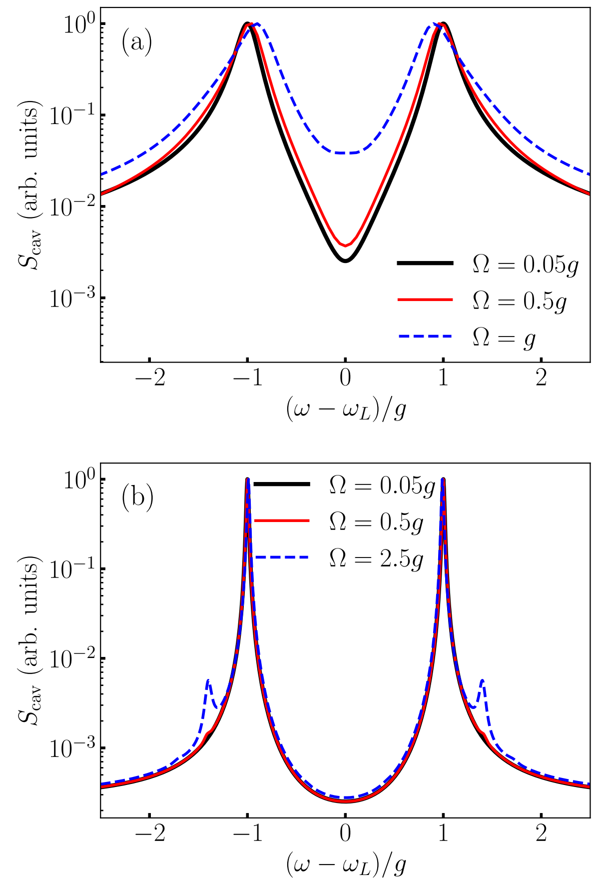

FIG. 8. Cavity-emitted spectra of the driven JC solution (single qubit-cavity system) for different qubit drive strengths [Eq. (30)], with $\kappa = \gamma_p$ (which yields equivalent broadening in the linear strong-coupling regime, in the Markov regime). (a) Driven system with $\kappa = \gamma_p$, to yield an equivalent linear polariton to the three-qubit system. (b) Solution with a smaller value of the decay rate $\kappa = 0.1\gamma_p$, where additional peaks can be partly observed for stronger pumps.

Although the lower two polariton states have an equivalence with the three-qubit system in the Markov regime (namely, both can yield vacuum Rabi oscillations), this is only for linear excitation. Clearly the nonlinear states are quite different, and it is also well known that accessing the higher-lying states of the JC system is notoriously difficult [34,35,58,59] and typically one needs very large g/κ ratios, e.g., with state-of-the-art circuit QED systems [33], or/and very specialized spectroscopy techniques. This makes the observation and exploitation of the nonlinear JC states very challenging. Part of the problem in the JC system is that the dissipation also scales with the photon number, causing increasing dissipation for the higher-lying excitations.

In order to compare our driven three-qubit results with the (dissipative) JC solution, we choose the same value of g and set $\kappa = \gamma_p$, since this yields similar polariton resonances with weak excitation (see Fig. 2). However, as can be seen in Fig. 8(a), the observable peaks in a JC system are too broad to allow any discernible features from higher-order spectral peaks. For clarity, we also show the solution with an order of magnitude reduction in the cavity decay rate, $\kappa = 0.1\gamma_p$;

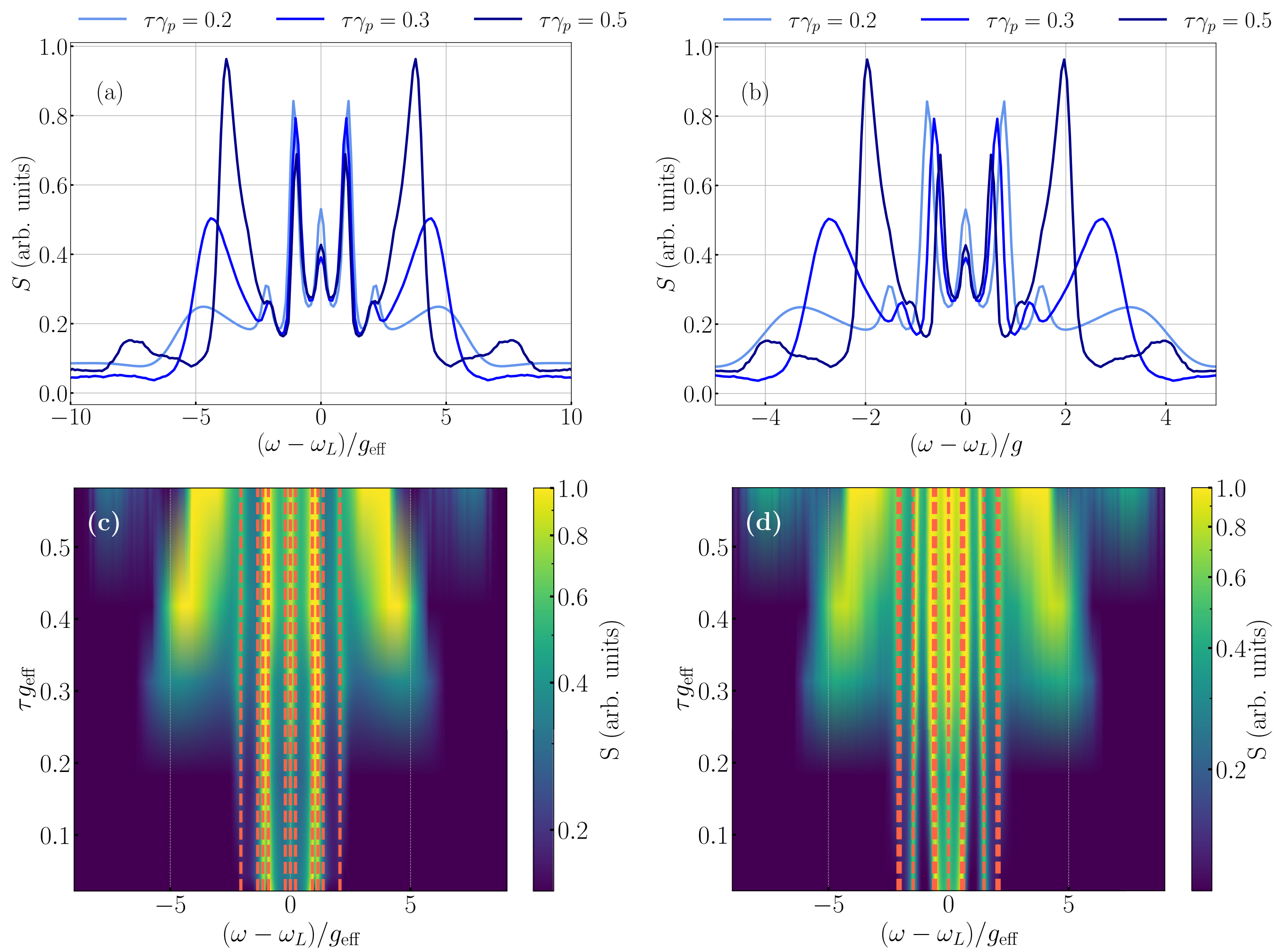

FIG. 9. Output spectra of a three-qubit system (with $\gamma_m/\gamma_p = 10$) calculated using the MPS approach with the probe dot pumped with $\Omega = 0.5\gamma_p$. Spectra with three delay times ($\tau\gamma_p = 0.2$, 0.3, and 0.5) are plotted as a function of (a) $(\omega - \omega_L)/g_{\rm eff}$ and (b) $(\omega - \omega_L)/g$. Note the different frequency scales. Also shown are contour plots with similar calculations of the output spectrum as a function of the delay times, with $\tau_{\rm max} = 0.5/\gamma_p$, for (c) on-resonance pumping and (d) off-resonance pumping with $\Delta_n = g_{\rm eff}/2$. Red dashed lines show the transition lines previously calculated in the Markovian regime.

in this case, we can partly observe some of the anharmonic ladder states [Fig. 8(b)], though these are rather weak, even on a logarithmic scale. To be clear, in Fig. 8(b), with suitable pumping, we barely observe a peak at $(\omega - \omega_L)/g = \sqrt{2}$, which corresponds to the second excitation manifold in Fig. 7, and an even smaller peak at $(\omega - \omega_L)/g = \sqrt{3}$, corresponding to the third excitation manifold (or fourth energy level in Fig. 7). This is significantly different from the results observed in Fig. 4, where for much weaker pump fields we can already see nonlinear spectral peaks representing different transitions between the dressed states of the three-qubit system, and these are all clearly resolved even on a linear scale.

Note that, in contrast to the dissipate JC system, in the three-qubit waveguide system there is no direct cavity decay: The full solution for photons and decay is automatically captured through the couplings between the qubits and waveguide modes; the side qubits act as mirrors and yield multiple cavity resonances, as discussed earlier, with the lower two polaritons having a decay rate of $\gamma_p/4$, which is analogous to a broadening of $\kappa/4$ only in the linear spectrum of a dissipative JC model [49].

C. Nonlinear non-Markovian regime

Next we investigate the non-Markovian regime making use of the MPS approach seen in Sec. II B. Here we fully account for the effects of retardation and nonlinearities on the pump-induced spectra.

In the nonlinear regime, the spectrum in the presence of retardation effects is shown in Fig. 9. We choose three example delay times (on-resonance) and plot the spectrum in terms of $g_{\rm eff}$ [Fig. 9(a)] and in terms of g [Fig. 9(b)]. We can observe how the peaks, which can be explained through the dressed energy ladder states, do not depend on the retardation when considered in terms of $g_{\rm eff}$, although they appear at different positions when computed in terms of g.

In Figs. 9(c) and 9(d) the output field spectra are calculated for various delay times with an on-resonance pump [Fig. 9(c)]

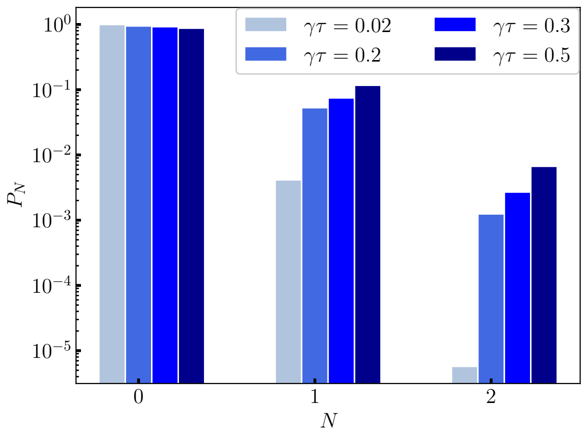

FIG. 10. Logarithmic scale of the photon probabilities for the first few photon states in the waveguide cavity region, for the case of resonant pumping (the case with off-resonant pumping is similar and thus is not shown).

and an off-resonance one with $\Delta_n = g_{\rm eff}/2$ [Fig. 9(d)], where $\Omega = 0.5\gamma_p$ in both cases. The spectral peaks seen in Fig. 6 are also observed in this regime. We recognize how these peaks do not depend on retardation as they appear as straight vertical lines. However, the splitting observed on-resonance in the Markovian regime disappears as the delay times increase. Also, note that the retardation-induced peaks become narrower for increased delay times.

In addition to the peaks identified from the Markovian dressed states, there are now some extra peaks that emerge for sufficiently large values of τ that cannot be explained in the Markovian limit, which also vary depending on the retardation (time delays). It is important to note that these additional resonances are not due to higher-order cavity modes, since the free spectral range on this system, defined as $\Delta\omega_{\rm FSR} \approx \frac{2\pi}{\tau_{\rm RT}\gamma_p}$, where $\tau_{\rm RT} = 2\tau$, is outside the frequency regime shown. For instance, for $\tau\gamma_p = 0.3$, $\Delta\omega_{\rm FSR} = 10.47\gamma_p$, which is outside the spectral limits in Fig. 9. Thus the additional nonlinear peaks with retardation are not related to higher-order (cavity-like) modes.

The retardation-induced new peaks move in frequency and get more pronounced as the delay time increases, suggesting that this is a purely non-Markovian effect. To help us understand the origin of these new peaks, we also calculate the photon probabilities P_N, by projecting the photon-number operators on each time bin and calculating the probability of having zero or one photon ($|0\rangle\langle 0|$ and $|1\rangle\langle 1|$, respectively) and combining these results to get the probability of having zero (P_0), one (P_1), and two (P_2) photons in the part of the waveguide confined between the mirror qubits. We investigate this for four different retardation values to see how they vary as a function of τ, for $\Omega = 0.5\gamma_p$ and $\Delta_n = 0$ (Fig. 10).

We observe that the probability of having two photons increases for higher values of τ, although it stays considerably low in all case studies (for both on- and off-resonance calculations). In all our simulations, we also observe significant photon bunching in our system, which becomes more pronounced for longer time delays.

A similar phenomenon was previously reported in Refs. [29,45], for time-delayed feedback, in the case of a single TLS in front of a mirror, where they found that new non-Markovian resonances appear at frequencies $\omega = (\phi + 2\pi\mathbb{Z})/\tau$, with $\mathbb{Z}$ the set of integers, ϕ the phase of the mirror, and τ the retardation time between the mirror and the TLS. In our system, we do not have a single phase since there are three different phases involved due to the interaction between the three qubits, but we can observe an analogous trend in the dependence of these new peaks with respect to the delay times. In addition, our qubits act as nonlinear TLSs and also have a frequency-dependent reflection, making the analysis more complicated than the single perfect mirror.

This supports the idea that the additional resonances we obtain with retardation are mediated through entangled photon-matter states not present in the Markovian master-equation solution (where the waveguide modes are traced out). Thus, it is essential here to have a method (such as the MPS approach) that treats the waveguide photons as part of the system, allowing for entangled photon matter states.

IV. CONCLUSIONS

We have presented a theoretical study of an optically pumped three-qubit waveguide system where the side qubits act as mirrors, creating a cavitylike system with a probe qubit in its center. We have theoretically modeled this system, starting with a linear model (for reference) and then accounted for various nonlinear interactions, where we studied the Markovian limit by solving the medium-dependent (waveguide-qubit) master equation. The Markovian regime allowed us to compare our results with a cavity system to establish a γ_m/γ_p ratio that resembles the cavity behavior with the same characteristic vacuum Rabi splitting and then with the well-known JC model. With optical pumping, we observed new resonances including four resonances with a splitting near the one-photon JC resonances, showing signatures of multiquantum effects beyond weak excitation.

The nonlinearities were further explained by computing the dressed energy levels, where we first connected the dressed state basis (in the absence of any optical pumping) with the bare state basis. Then we added an optical pump field and computed again the dressed energy levels, as well as the dressed-state populations, and subsequently the spectral peaks with their corresponding transitions. For comparison, we also showed the first few nonlinear states of a driven JC system, which was shown to yield a drastically different nonlinear response. Moreover, the higher-order resonances of the driven JC system were not visible with a comparable level of dissipation.

Finally, we extended the model to include retardation and non-Markovian dynamics, solving the Hamiltonian with the MPS approach and comparing results for various values of time retardation. We observed how the resonances previously identified in the Markovian limit do not depend on retardation if shown in terms of an effective coupling rate $g_{\rm eff}$. We then found additional peaks that cannot be seen in the Markovian regime at all, which depend on the delay times; these peaks become narrower for higher delay times (which is a purely non-Markovian effect). Photon probabilities were also calculated with the MPS method, showing low values of the two photon probabilities (although in an increasing trend with longer retardation times). These new resonances stem from additional waveguide photon-matter states, which cannot be seen in the Markovian regime.

ACKNOWLEDGMENTS

This work was supported by the Natural Sciences and Engineering Research Council of Canada, the National Research Council of Canada, the Canadian Foundation for Innovation, and Queen's University, Canada.

[1] A. Blais, A. L. Grimsmo, S. M. Girvin, and A. Wallraff, Circuit quantum electrodynamics, Rev. Mod. Phys. **93**, 025005 (2021).
[2] J.-T. Shen and S. Fan, Strongly correlated multiparticle transport in one dimension through a quantum impurity, Phys. Rev. A **76**, 062709 (2007).
[3] D. Roy, C. M. Wilson, and O. Firstenberg, Colloquium: Strongly interacting photons in one-dimensional continuum, Rev. Mod. Phys. **89**, 021001 (2017).
[4] A. S. Sheremet, M. I. Petrov, I. V. Iorsh, A. V. Poshakinskiy, and A. N. Poddubny, Waveguide quantum electrodynamics: Collective radiance and photon-photon correlations, Rev. Mod. Phys. **95**, 015002 (2023).
[5] J. Román-Roche, E. Sánchez-Burillo, and D. Zueco, Bound states in ultrastrong waveguide QED, Phys. Rev. A **102**, 023702 (2020).
[6] S. J. Masson and A. Asenjo-Garcia, Atomic-waveguide quantum electrodynamics, Phys. Rev. Res. **2**, 043213 (2020).
[7] S. Mahmoodian, M. Čepulkovskis, S. Das, P. Lodahl, K. Hammerer, and A. S. Sørensen, Strongly Correlated Photon Transport in Waveguide Quantum Electrodynamics with Weakly Coupled Emitters, Phys. Rev. Lett. **121**, 143601 (2018).
[8] N. Liu, X. Wang, X. Wang, X.-S. Ma, and M.-T. Cheng, Tunable single photon nonreciprocal scattering based on giant atom-waveguide chiral couplings, Opt. Express **30**, 23428 (2022).
[9] L. Du, Y. Zhang, J.-H. Wu, A. F. Kockum, and Y. Li, Giant Atoms in a Synthetic Frequency Dimension, Phys. Rev. Lett. **128**, 223602 (2022).
[10] D. D. Noachtar, J. Knörzer, and R. H. Jonsson, Nonperturbative treatment of giant atoms using chain transformations, Phys. Rev. A **106**, 013702 (2022).
[11] C. Wang, X.-S. Ma, and M.-T. Cheng, Giant atom-mediated single photon routing between two waveguides, Opt. Express **29**, 40116 (2021).
[12] A. F. Kockum, G. Johansson, and F. Nori, Decoherence-Free Interaction between Giant Atoms in Waveguide Quantum Electrodynamics, Phys. Rev. Lett. **120**, 140404 (2018).
[13] B. Kannan, M. J. Ruckriegel, D. L. Campbell, A. F. Kockum, J. Braumüller, D. K. Kim, M. Kjaergaard, P. Krantz, A. Melville, B. M. Niedzielski, A. Vepsäläinen, R. Winik, J. L. Yoder, F. Nori, T. P. Orlando, S. Gustavsson, and W. D. Oliver, Waveguide quantum electrodynamics with superconducting artificial giant atoms, Nature (London) **583**, 775 (2020).
[14] A. Carollo, D. Cilluffo, and F. Ciccarello, Mechanism of decoherence-free coupling between giant atoms, Phys. Rev. Res. **2**, 043184 (2020).
[15] M. Mirhosseini, E. Kim, X. Zhang, A. Sipahigil, P. B. Dieterle, A. J. Keller, A. Asenjo-Garcia, D. E. Chang, and O. Painter, Cavity quantum electrodynamics with atom-like mirrors, Nature (London) **569**, 692 (2019).
[16] S. J. Masson and A. Asenjo-Garcia, Darkness tamed with superconducting qubits, Nat. Phys. **18**, 490 (2022).
[17] A. Laucht, S. Pütz, T. Günthner, N. Hauke, R. Saive, S. Frédérick, M. Bichler, M.-C. Amann, A. W. Holleitner, M. Kaniber, and J. J. Finley, A Waveguide-Coupled On-Chip Single-Photon Source, Phys. Rev. X **2**, 011014 (2012).
[18] V. S. C. Manga Rao and S. Hughes, Single quantum-dot Purcell factor and β factor in a photonic crystal waveguide, Phys. Rev. B **75**, 205437 (2007).
[19] T. Lund-Hansen, S. Stobbe, B. Julsgaard, H. Thyrrestrup, T. Sünner, M. Kamp, A. Forchel, and P. Lodahl, Experimental Realization of Highly Efficient Broadband Coupling of Single Quantum Dots to a Photonic Crystal Waveguide, Phys. Rev. Lett. **101**, 113903 (2008).
[20] M.-T. Cheng, J. Xu, and G. S. Agarwal, Waveguide transport mediated by strong coupling with atoms, Phys. Rev. A **95**, 053807 (2017).
[21] G. Crowder, H. Carmichael, and S. Hughes, Quantum trajectory theory of few-photon cavity-QED systems with a time-delayed coherent feedback, Phys. Rev. A **101**, 023807 (2020).
[22] K. Sinha, P. Meystre, E. A. Goldschmidt, F. K. Fatemi, S. L. Rolston, and P. Solano, Non-Markovian Collective Emission from Macroscopically Separated Emitters, Phys. Rev. Lett. **124**, 043603 (2020).
[23] S. Arranz Regidor, G. Crowder, H. Carmichael, and S. Hughes, Modeling quantum light-matter interactions in waveguide QED with retardation, nonlinear interactions, and a time-delayed feedback: Matrix product states versus a space-discretized waveguide model, Phys. Rev. Res. **3**, 023030 (2021).
[24] A. Carmele, J. Kabuss, F. Schulze, S. Reitzenstein, and A. Knorr, Single Photon Delayed Feedback: A Way to Stabilize Intrinsic Quantum Cavity Electrodynamics, Phys. Rev. Lett. **110**, 013601 (2013).
[25] A. L. Grimsmo, Time-Delayed Quantum Feedback Control, Phys. Rev. Lett. **115**, 060402 (2015).
[26] S. J. Whalen, A. L. Grimsmo, and H. J. Carmichael, Open quantum systems with delayed coherent feedback, Quantum Sci. Technol. **2**, 044008 (2017).
[27] G. Calajó, Y.-L. L. Fang, H. U. Baranger, and F. Ciccarello, Exciting a Bound State in the Continuum through Multiphoton Scattering Plus Delayed Quantum Feedback, Phys. Rev. Lett. **122**, 073601 (2019).
[28] C. A. González-Gutiérrez, J. Román-Roche, and D. Zueco, Distant emitters in ultrastrong waveguide QED: Ground-state properties and non-Markovian dynamics, Phys. Rev. A **104**, 053701 (2021).
[29] G. Crowder, L. Ramunno, and S. Hughes, Quantum trajectory theory and simulations of nonlinear spectra and multiphoton effects in waveguide-QED systems with a time-delayed coherent feedback, Phys. Rev. A **106**, 013714 (2022).

[30] K. Barkemeyer, A. Knorr, and A. Carmele, Heisenberg treatment of multiphoton pulses in waveguide QED with time-delayed feedback, Phys. Rev. A **106**, 023708 (2022).
[31] K. Sinha, A. González-Tudela, Y. Lu, and P. Solano, Collective radiation from distant emitters, Phys. Rev. A **102**, 043718 (2020).
[32] L. S. Bishop, J. M. Chow, J. Koch, A. A. Houck, M. H. Devoret, E. Thuneberg, S. M. Girvin, and R. J. Schoelkopf, Nonlinear response of the vacuum Rabi resonance, Nat. Phys. **5**, 105 (2009).
[33] J. M. Fink, M. Göppl, M. Baur, R. Bianchetti, P. J. Leek, A. Blais, and A. Wallraff, Climbing the Jaynes–Cummings ladder and observing its nonlinearity in a cavity QED system, Nature (London) **454**, 315 (2008).
[34] I. Schuster, A. Kubanek, A. Fuhrmanek, T. Puppe, P. W. H. Pinkse, K. Murr, and G. Rempe, Nonlinear spectroscopy of photons bound to one atom, Nat. Phys. **4**, 382 (2008).
[35] E. Illes, C. Roy, and S. Hughes, Spectral multiphoton effects and quantum anharmonicities in dissipative cavity-QED systems via off-resonant coherent excitation, Optica **2**, 689 (2015).
[36] G. S. Agarwal, Vacuum-field Rabi oscillations of atoms in a cavity, J. Opt. Soc. Am. B **2**, 480 (1985).
[37] Y. Zhu, D. J. Gauthier, S. E. Morin, Q. Wu, H. J. Carmichael, and T. W. Mossberg, Vacuum Rabi Splitting as a Feature of Linear-Dispersion Theory: Analysis and Experimental Observations, Phys. Rev. Lett. **64**, 2499 (1990).
[38] D. E. Chang, L. Jiang, A. V. Gorshkov, and H. J. Kimble, Cavity QED with atomic mirrors, New J. Phys. **14**, 063003 (2012).
[39] C. Zhou, Z. Liao, and M. S. Zubairy, Decay of a single photon in a cavity with atomic mirrors, Phys. Rev. A **105**, 033705 (2022).
[40] S. Arranz Regidor and S. Hughes, Cavitylike strong coupling in macroscopic waveguide QED using three coupled qubits in the deep non-Markovian regime, Phys. Rev. A **104**, L031701 (2021).
[41] H. T. Dung, L. Knöll, and D.-G. Welsch, Resonant dipole-dipole interaction in the presence of dispersing and absorbing surroundings, Phys. Rev. A **66**, 063810 (2002).
[42] G. Angelatos and S. Hughes, Entanglement dynamics and Mollow nonuplets between two coupled quantum dots in a nanowire photonic-crystal system, Phys. Rev. A **91**, 051803(R) (2015).
[43] G. S. Agarwal, Quantum electrodynamics in the presence of dielectrics and conductors. IV. General theory for spontaneous emission in finite geometries, Phys. Rev. A **12**, 1475 (1975).
[44] G. S. Agarwal, *The Jaynes-Cummings Model and Its Descendants* (Cambridge University Press, Cambridge, 2013).
[45] H. Pichler and P. Zoller, Photonic Circuits with Time Delays and Quantum Feedback, Phys. Rev. Lett. **116**, 093601 (2016).
[46] A. Carmele, N. Nemet, V. Canela, and S. Parkins, Pronounced non-Markovian features in multiply excited, multiple emitter waveguide QED: Retardation induced anomalous population trapping, Phys. Rev. Res. **2**, 013238 (2020).
[47] A. B. Young, A. C. T. Thijssen, D. M. Beggs, P. Androvitsaneas, L. Kuipers, J. G. Rarity, S. Hughes, and R. Oulton, Polarization Engineering in Photonic Crystal Waveguides for Spin-Photon Entanglers, Phys. Rev. Lett. **115**, 153901 (2015).
[48] I. Söllner, S. Mahmoodian, S. L. Hansen, L. Midolo, A. Javadi, G. Kiršanskė, T. Pregnolato, H. El-Ella, E. H. Lee, J. D. Song, S. Stobbe, and P. Lodahl, Deterministic photon–emitter coupling in chiral photonic circuits, Nat. Nanotechnol. **10**, 775 (2015).
[49] L. C. Andreani, G. Panzarini, and J.-M. Gérard, Strong-coupling regime for quantum boxes in pillar microcavities: Theory, Phys. Rev. B **60**, 13276 (1999).
[50] K. Mnaymneh, D. Dalacu, J. McKee, J. Lapointe, S. Haffouz, J. F. Weber, D. B. Northeast, P. J. Poole, G. C. Aers, and R. L. Williams, On-chip integration of single photon sources via evanescent coupling of tapered nanowires to SiN waveguides, Adv. Quantum Technol. **3**, 1900021 (2019).
[51] J. R. Johansson, P. D. Nation, and F. Nori, QuTiP: An open-source Python framework for the dynamics of open quantum systems, Comput. Phys. Commun. **183**, 1760 (2012).
[52] J. R. Johansson, P. D. Nation, and F. Nori, QuTiP 2: A Python framework for the dynamics of open quantum systems, Comput. Phys. Commun. **184**, 1234 (2013).
[53] O. Astafiev, A. M. Zagoskin, A. A. Abdumalikov, Jr., Y. A. Pashkin, T. Yamamoto, K. Inomata, Y. Nakamura, and J. S. Tsai, Resonance fluorescence of a single artificial atom, Science **327**, 840 (2010).
[54] M. Florescu and S. John, Resonance fluorescence in photonic band gap waveguide architectures: Engineering the vacuum for all-optical switching, Phys. Rev. A **69**, 053810 (2004).
[55] C. Gustin, R. Manson, and S. Hughes, Spectral asymmetries in the resonance fluorescence of two-level systems under pulsed excitation, Opt. Lett. **43**, 779 (2018).
[56] E. Jaynes and F. Cummings, Comparison of quantum and semi-classical radiation theories with application to the beam maser, Proc. IEEE **51**, 89 (1963).
[57] H. J. Carmichael, R. J. Brecha, M. G. Raizen, H. J. Kimble, and P. R. Rice, Subnatural linewidth averaging for coupled atomic and cavity-mode oscillators, Phys. Rev. A **40**, 5516 (1989).
[58] J. Kasprzak, S. Reitzenstein, E. A. Muljarov, C. Kistner, C. Schneider, M. Strauss, S. Höfling, A. Forchel, and W. Langbein, Up on the Jaynes–Cummings ladder of a quantum-dot/microcavity system, Nat. Mater. **9**, 304 (2010).
[59] J. Larson and T. Mavrogordatos, *The Jaynes-Cummings Model and Its Descendants* (IOP, Bristol, 2021).